Author Manuscript

Author Manuscript

Author Manuscript

Author Manuscript

HHS Public Access

Author manuscript

Brain Stimul. Author manuscript; available in PMC 2020 November 01.

Published in final edited form as:

Brain Stimul. 2019 ; 12(6): 1439–1447. doi:10.1016/j.brs.2019.07.015.

Reversible neuroinhibition by focused ultrasound is mediated by a thermal mechanism

David P. Darrow[a,*], **Parker O'Brien**[b], **Thomas J. Richner**[c], **Theoden I. Netoff**[c], **Emad S. Ebbini**[b]

[a]Department of Neurosurgery, University of Minnesota, MMC 96, Room D-429, 420 Delaware St SE, Minneapolis, MN, 55455, USA

[b]Department of Electrical and Computer Engineering, University of Minnesota, 7-174 Keller Hall, 200 Union Street Se. Minneapolis, MN, 55455, USA

[c]Department of Biomedical Engineering, University of Minnesota, 7-105 Nils Hasselmo Hall, 312 Church St. SE, Minneapolis, MN, 55455, USA

Abstract

Background: Transcranial focused ultrasound (tFUS) at low intensities has been reported to directly evoke responses and reversibly inhibit function in the central nervous system. While some doubt has been cast on the ability of ultrasound to directly evoke neuronal responses, spatially-restricted transcranial ultrasound has demonstrated consistent, inhibitory effects, but the underlying mechanism of reversible suppression in the central nervous system is not well understood.

Objective/hypothesis: In this study, we sought to characterize the effect of transcranial, low-intensity, focused ultrasound on the thalamus during somatosensory evoked potentials (SSEP) and investigate the mechanism by modulating the parameters of ultrasound.

Methods: TFUS was applied to the ventral posterolateral nucleus of the thalamus of a rodent while electrically stimulating the tibial nerve to induce an SSEP. Thermal changes were also induced through an optical fiber that was image-guided to the same target.

Results: Focused ultrasound reversibly suppressed SSEPs in a spatially and intensity-dependent manner while remaining independent of duty cycle, peak pressure, or modulation frequency. Suppression was highly correlated and temporally consistent with *in vivo* temperature changes while producing no pathological changes on histology. Furthermore, stereotactically-guided delivery of thermal energy through an optical fiber produced similar thermal effects and suppression.

Conclusion: We confirm that tFUS predominantly causes neuroinhibition and conclude that the most primary biophysical mechanism is the thermal effect of focused ultrasound.

*Corresponding author. darro015@umn.edu (D.P. Darrow).

Conflicts of interest

A provisional patent application (U.S. 62/738,420) has been filed concerning the technology presented in this work.

Appendix A. Supplementary data

Supplementary data to this article can be found online at https://doi.org/10.1016Zj.brs.2019.07.015.

Author Manuscript Author Manuscript Author Manuscript Author Manuscript

Keywords

Transcranial focused ultrasound; Low intensity; Noninvasive; FUS; Somatosensory evoked potentials; Neuromodulation

Introduction

Reversible neuromodulation using ultrasound through a craniotomy was first reported more than 60 years ago. [1] Since then, the promise of a noninvasive method of using mechanical waves to modulate the function of the nervous system with submillimeter resolution has been fueled by substantial improvements in modeling, ultrasound transducer design, and computational power. [2–4] Compared to existing noninvasive neuromodulation platforms such as transcranial magnetic stimulation (TMS) and transcranial direct current stimulation (tcDCS), tFUS has superior spatial resolution. [3].

The skull is highly reflective, diffractive, and absorptive of ultrasound, producing a significant barrier to delivery of ultrasound to the brain, and these effects can vary widely across regions of the skull with differing thickness and concavity. [5–8] Transcranial focused ultrasound (tFUS) incorporates strategies to account for these effects in order to minimize distortion. [4,5] Phased arrays of ultrasound transducers and modeling techniques make it possible to take into account the anatomical variation in order to focus ultrasound through the skull while distributing energy delivery across the scalp. [6] The dual-mode ultrasound array (DMUA) technology is a new paradigm in image-guided FUS interventions enabling simultaneous delivery of high resolution therapy while actively monitoring the sonicated tissue. [9–11] Real-time monitoring, such as ultrasound thermography, enables imaging of the temperature of the tissue heated by ultrasound and can be performed in closed-loop fashion to adjust for distortion. [5,12] Our group previously demonstrated that this technique successfully produces localized effects in a rodent model through monitoring of tFUS-induced subtherapeutic heating of brain tissues. [5] In addition to its basic (3D) image guidance capabilities, our DMUA system employs advanced multi-channel transmit control circuitry allowing investigation over a large parameter space.

While tFUS at high intensities can open the blood-brain barrier, or create lesions to ablate tumors, tFUS at lower intensities has been reported to reversibly modulate neural activity without damaging tissue. [13–15] Inhibition and excitation by tFUS have been reported in *in vitro, in vivo* in animals, in and humans. [3] The reported effects of transcranial tFUS range from evoked neural activity to modulation of sensory evoked-potentials. [8,16–24] Numerous mechanisms have been suggested based on the interaction between known ultrasound biophysical effects and neuro-physiology, but the heterogeneity of effects and experimental confounds shroud our understanding of the main underlying mechanisms. [3].

A common tFUS experimental paradigm uses a laterally-restricted ultrasound focus from a single element transducer where the ventral-dorsal extent of the ultrasound beam spans the entire skull of the animal. [25] Recently, a pair of studies highlighted an important confound in this paradigm, where it was shown that delivery of ultrasound in this way results in tFUS beams with a large dorsoventral area of effect, directing ultrasound into the base of the skull

Author Manuscript Author Manuscript Author Manuscript Author Manuscript

to the cochlea and inner ear and therefore produces an auditory-startle response. [26,27]. This may explain, at least in part, some of the ultrasound-evoked responses previously reported. [26,27] In contrast, experiments using phased-arrays capable of restricting the ultrasound focus in all three dimensions, or in humans where the skull base remains far from the focus, report inhibitory effects on active neural circuits. [8,15,17,23] Considerable uncertainty remains regarding the mechanism of inhibition as ultrasound produces several effects within biological tissue including thermal effects and mechanical effects, such as radiation pressure, shear waves, cavitation, and microcavitation. [2,28].

Here we sought to characterize the effect of tFUS at low-intensities on a well-characterized neural circuit: the primary somatosensory afferent pathway. In this study we vary the parameters of the ultrasound beam and measure each parameter's effects on modulating the pathway to elucidate the underlying mechanism.

Methods

Ultrasound system

A 64-element DMUA transducer was used for transcranial imaging and delivery of tFUS neuromodulation. [5] The array was driven by a 32-channel linear amplifier with programmable independent waveforms in both imaging and therapy modes. The arbitrary driving waveforms were synthesized based on the desired target (focus) point and modulation scheme using previously described focusing algorithms. [11] A custom designed MATLAB (R2016a, The MathWorks, Inc., Natick, Massachusetts) interface was used to download the waveforms to a custom FPGA front end, described in Casper et al. [9].

Ultrasound imaging

Two DMUA imaging modes, described previously, were used. [11,29] Briefly, synthetic aperture (SA) imaging mode was used for guidance and localization of tFUS. Single transmit focus (STF) imaging was used for monitoring of tFUS application and to characterize its thermal and mechanical bioeffects. STF is a high speed imaging mode that allowed for monitoring the tissue response to tFUS at hundreds of frames per second.

Ultrasound characterization

Power and intensities were measured in a degassed water bath with and without ex-vivo skulls using an Onda hydrophone (Onda Corporation, Sunnyvale, CA). Field scans were performed in planes parallel to the surface of the DMUA in the focal plane of the intended focus, i.e. to measure a cross section of the focal spot. This was done using a fine grid with spacing smaller than $\lambda/3$, where λ is the wavelength of the tFUS beam. The extent of the scan was large enough to capture the 2D extent of the focal spot and the significant sidelobes in the lateral and elevation directions. Using calibration tables provided by the vendor, this allowed the use of the hydro-phone measurements to compute the acoustic pressure, intensity and integrated power.

Author Manuscript Author Manuscript Author Manuscript Author Manuscript

Ultrasound thermography

Briefly, 1-sec test tFUS shots were delivered to the target at intensity levels similar to those used in the neuromodulation experiments described in this paper. Real-time DMUA imaging data was collected 1 s before, during, and 8 s after tFUS at 200 frames per second. The signal processing algorithm described in Ebbini et al. [30] was used to evaluate the temperature change profiles resulting from the application of the 1-sec test shots.

Temperature characterization

A type-T (copper-constantan) 200 mm hypodermic needle thermocouple (Type-0, Omega Engineering, Norwalk, CT) was used for localized measurement of temperature at the target location. The temperature values were measured at a rate of 100 Hz using Agilent 34970A data acquisition unit (Agilent Technologies, Santa Clara, CA).

Stereotaxis and 3D rendering

A Daedal *xyz*-stage computer-controlled stepper-motor system (Parker-Hannifan, Cleveland, OH) with precise three-dimensional control was used. The *xyz*-stage was used to obtain sequential coronal SA DMUA images. A custom designed FPGA controller was used to synchronize the motion position with the SA frame count to allow for 3D rendering of the volume scan data. Transverse planes corresponding to C-mode ultrasound scan were extracted for identification of the suture lines, which were used as reference for precise placement of the tFUS beam using a method of stereotaxis previously described. [31] Three-dimensional DMUA imaging was used to position the focus at precise stereotactic coordinates with respect to the skull sutures, which were easily identifiable with imaging (see Fig. 2d). We targeted the ultrasound focus to the ventral posterior lateral (VPL) nucleus of the thalamus (3 mm posterior to Bregma, 3 mm lateral, 6 mm deep to cortex). [32].

SSEP experimental procedure

In accordance with a UMN-approved IACUC protocol, Sprague-Dawley (obtained from Charles River Laboratories) rats (n = 15) between 250 g and 350 g were anesthetized with a ketamine (40–90 mg/kg) and xylazine (5–10 mg/kg) delivered IP until complete suppression of motor response to deep toe pinch. Maintenance injections of ketamine (20 mg/kg) were delivered if a toe pinch response was measured. This combination of a dissociative with an alpha-2 agonist has a minimal effect on the transmission of sensory information. [3] No effort was made to lighten anesthesia. The head was rigidly fixed with ear bars, and 1 cc of 1% lidocaine with 1:100000 epinephrine was used for local anesthetic. The scalp was incised and periosteum cleared. One mm burr holes were placed bilaterally at 2 mm posterior and 2 mm lateral to Bregma. Epidural potentials were measured via the burr holes using shielded stainless steel wire with differential source from a midline subcutaneous frontal electrode and separately grounded subcutaneously. Signals were amplified 100× and bandpass filtered between 0.1 Hz and 3 kHz using Grass P511 amplifiers. Signals were then digitized at 10 kHz using a National Instruments (Austin, Texas) 16-bit digitizer. Data was recorded using open source Real-Time eXperimental Interface software. [33] The tibial nerve was stimulated after insertion of subcutaneous needles, using a voltage-controlled GRASS (S88, Grass Astro-Med, W. Warwick, RI) stimulator at 4.3 Hz and pulse width of

Author Manuscript Author Manuscript Author Manuscript Author Manuscript

600 μsec A voltage between 0.5 and 3 V was tailored to generate the minimal suprathreshold stimulation.

Experimental epochs consisted of 120 s of baseline SSEP followed by 150 s of SSEP during ultrasound stimulation, which was followed by a 60 s washout period. Baseline SSEP measurements were taken to calculate 10 sequential periods of 50 SSEP windows. Ultrasound was delivered for 30 s followed by 10 sequential periods of 50 SSEP windows. Average SSEP waveforms were calculated during each period. Peak-to-peak measurements were computed for each period. To provide a conservative estimate of ultrasound's effect on the SSEP, the ratio of every combination of baseline and therapy windows were calculated and used as the distribution to determine the effect size across ultrasound parameters.

Laser heating

A 50 mW laser of 650 nm (Visual Fault Locator, J-Deal TL532) was used to deliver light through a 100 μm fiberoptic cable. Incident light calibration measured 35 mW at the distal tip.

Statistical analysis

The Kolmogorov-Smirnov Test was used to compare groups of data. Alpha was selected to be 0.05 with Bonferroni correction for multiple comparisons.

Results

Ultrasound characterization

A 64-element DMUA prototype was used to generate modulated tFUS patterns in the thalamus, Fig. 1. The transmitted FUS field patterns were first measured in degassed water. Measurements were made using a 3.2 MHz carrier frequency, 50 kHz modulation frequency, and pulse-repetition frequency of 500 Hz (waveform in Appendix A). Reference focal plane patterns were measured on a grid with 0.05 (medial-latera)l × 0.1 (elevation) mm^2, Fig. 2 (a and c). In each experiment, a 3D image of the skull surface was obtained by mechanically scanning the DMUA while collecting 2D pulse-echo data in synthetic aperture (SA) imaging mode. [31] To characterize beam distortion due to skull interference, the field patterns were measured transcranially on the same focal plane grid using five skull samples. These measurements revealed significant loss in transmitted power due to absorption by the skull, consistent with previously reports. [34] Fig. 2b demonstrates the focus below the skull in a coronal section. On average, 15% of the FUS beam peak power (8 dB loss with variance of 1.3 dB) was transmitted through the skull to the target location. The width of the beam at 3 dB reduction from the peak power was found to be deformed (from a resolution of 0.5 mm lateral diameter by 1 mm in the orthogonal direction in water) to 1 mm in the lateral direction by 2.5 mm in the orthogonal direction at the stereotactic coordinates of the VPL. In addition, defocusing effects were evident in some cases, including split focusing. More examples are shown in Appendix A.

Real-time ultrasound thermography was used to measure the temperature and spatial-temporal evolution due to tFUS *in vivo*, similar to previous descriptions. [30] Fig. 3a shows

Author Manuscript Author Manuscript Author Manuscript Author Manuscript

the heating rate of the tFUS beam, which is indicative of the spatial intensity distribution in coronal section. Fig. 3b illustrates the time-evolution of the temperature field with respect to tFUS-on time. The temperature profiles demonstrate the spatial localization of tFUS-induced heating consistent with intensity profiles shown in Fig. 2 and the distortion patterns shown in Fig. A2. Specifically, the maximum tFUS-induced heating occurs ~1 mm prefocally (due to the lensing effect of the skull) with an extent of approximately 3 mm in the beam direction. The heated region has a classic "tadpole" shape with the extent of the heated region in the orthogonal direction of approximately 2.4 mm at the widest point. To confirm thermal response, we systematically evaluated the thermal effect *in vivo* across a broad range of ultrasound amplitudes and duty cycles using a fine-needle thermocouple temperature probe. A temperature response surface was interpolated, as shown in Fig. 3c. As expected, the temperature increased with the square of the amplitude of the ultrasound and linearly with the duty cycle. The change in temperature was highly correlated (Spearman R = 0.96) with the spatial peak temporal average intensity, I_{SPTA}, Fig. 3d.

tFUS modulation of SSEP amplitude

To assess the functional effects of ultrasound on neural activity, we measured SSEPs in the rat somatosensory cortex elicited by electrical stimulation applied to the contralateral tibial nerve while systematically applying tFUS to the ventral posterior lateral (VPL) nucleus of the thalamus. Rats were deeply anesthetized until they did not respond to toe pinch. No evoked or spontaneous movement was ever observed during the experiments or during ultrasound delivery. Tibial nerve stimulation produced large-amplitude SSEPs measured epidurally over the contralateral hemisphere. Averaging 50 SSEP traces produced highly-resolved evoked potential wave-forms with three dominant peaks (local maxima) (Fig. 4a/c). The first two peaks, P1 and P2, were reliable across animals, while the third peak, P3, was variable and not present in all animals. [35].

Ultrasound profoundly suppressed the SSEP waveform when focused on the VPL contralateral to the stimulated tibial nerve through which sensory signals for the stimulated pass. Near-complete suppression was achieved at an I_{SPTA} of 88 W/cm^2 (Fig. 4a). Ultrasound focused on the opposite VPL nucleus, ipsilateral to tibial nerve stimulation, had no effect when compared to baseline. The effect of ultrasound was not immediate, taking about 20 s to achieve maximal effect. The effect of ultrasound on the peak-to-peak amplitude of the SSEP (P1 to P2) over time is shown in Fig. 4b. Recovery of the SSEP after cessation of ultrasound was complete after approximately 20 s. No ultrasound-evoked responses were observed and no changes in the power spectra were found (see Appendix A).

US intensity determines SSEP suppression

We next characterized the effect of energy, by systematically varying the ultrasound amplitude (peak pressure) on SSEP amplitude relative to baseline. Suppression varied with I_{SPTA} (Fig. 4c). The effect of SPTA power, P_{SPTA}, on SSEP suppression relative to baseline amplitude fit well with a sigmoid curve (Fig. 4d). Statistically significant differences between each power and every other power were found ($p < 0.0001$) except between the smallest two. Specifically, at powers approaching zero, the peak-to-peak SSEP amplitude

Author Manuscript Author Manuscript Author Manuscript Author Manuscript

normalized to baseline approached 1. Suppression of the SSEP saturated at around 15 dB W/cm^2.

We delivered ultrasound stimulation over a range of duty cycles while adjusting the amplitude to keep the I_{SPTA} at a constant 20 W/cm^2 intensity to assess the effect of duty cycle and amplitude on the SSEP suppression. The effect of FUS at a constant I_{SPTA} was relatively unchanged for duty cycles from 5% to 70% (Fig. 5). No significant correlation between duty cycle (or the corresponding peak pressure) and SSEP normalized to baseline was found ($R^2 < .02$). The lack of relationship between suppression and duty cycle when I_{SPTA} is held constant suggests a mechanism linked closely to the time averaged intensity rather than an independent effect from duty cycle. Various modulation frequencies were also tested at two different intensities and found to have no significant effect on suppression (see Appendix A for details).

Temporal dynamics of ultrasound suppression of SSEP

The effect of FUS on the suppression of the SSEP was not instantaneous, persisting for tens of seconds beyond the ultrasound, which is long for a neural mechanism. Given the high correlation between I_{SPTA} and *in vivo* temperature changes in the focus (see Fig. 3d) we could infer the temperature changes during the application of ultrasound at three intensities, shown in Fig. 6a. The time course of SSEP suppression by tFUS was similar to that of the change in target temperature over time, Fig. 6 (Right), suggesting that temperature effects caused by ultrasound may be the primary mechanism of neuroinhibition.

Neuromodulation with laser heating

To isolate the effect of neuroinhibition by thermal energy, a laser was used to apply thermal energy through a fiber optic catheter to the VPL using the same SSEP experimental paradigm. To characterize the thermal effects of the laser, a fine-wire thermocouple probe placed under image guidance to allow direct assessment of the production of heat by the laser delivered through an optical fiber. The optical fiber was stereotactically placed along a vertical trajectory to the VPL where an optimal distance was experimentally obtained (information in Appendix A). The red light laser had an absorptive volume comparable to that of tFUS. The time course of the temperature at the tip of the optical fiber in the brain is plotted in Fig. 7a. Similar to the ultrasound experiments, a 2 °C rise was observed and SSEP amplitude suppressed to about 70% of steady state within 20 s. The resulting average waveforms (Fig. 7b) revealed profound suppression of the peak-to-peak amplitude between P1 and P2, similar to that seen with the ultrasound ($p < 0.00003$). The time course of suppression, as shown in Fig. 7c, was also similar to ultrasound suppression, supporting the hypothesis that the dominant effect of ultrasound is due to heating.

Histology

A subset of animals underwent repeated treatment across a range of intensities and were allowed to recover. No animals showed chronic behavioral effects. After 3–7 days the animals were sacrificed, brains were extracted and underwent histological examination using Hematoxylin and Eosin (H&E) staining (example results shown in Appendix A). Full sets of histology slides were reviewed by 3 qualified pathologists (H Brent Clark, Director of

Author Manuscript Author Manuscript Author Manuscript Author Manuscript

Neuropathology; Flaviu Tabaran and Gerrald O'Sullivan from Comparative Pathology Shared Resource). No pathological effects of the delivered ultrasound were found (Fig. A6).

Discussion

Low-intensity, focused, transcranial ultrasound is an ideal modality for reversible neuromodulation with high temporal and spatial resolution. Having the ability to inhibit specific neural circuits noninvasively could supplant existing neuromodulation platforms and provide unprecedented access to discover new treatments and understand functional connectivity of the brain *in vivo*. Despite the variety of reported effects and proposed mechanisms of FUS neuromodulation, uncertainty has remained. Here we demonstrate and confirm that low-intensity focused ultrasound can be used to suppress a primary sensory pathway by applying it to the thalamus in a rodent.

Our goal in this study was to clarify and unify observations across different frequencies and pulse widths and to find parameters of sinusoidal US optimized for neuroinhibition. The dual-mode ultrasound enables exploration of the effects of ultrasound on the rodent SSEP. We used a carrier frequency of 3.2 MHz in our DMUA system allowing an unprecedented level of localization over single transducer systems working at lower frequencies. [36] In addition, the DMUA transducer is highly concave, which reduces the size of the tFUS focus to a fraction of a millimeter in the lateral direction and approximately 2 mm in the dorsoventral (axial) direction. Distortion from the skull extends the focal spot size in the lateral-elevation dimensions, but even with these distortions the focal spot is a fraction of that used by others, which can be the size of 3.5 mm lateral and 6.2 mm along the beam axis. [36] Volumized ultrasound scans enabled precision focusing at stereotactic targets and the registration of imaging with therapy. This offers a distinct advantage when it comes to the placement of the tFUS beam with reference to the target as well as monitoring its effects, e.g. through real-time thermography. To the best of our knowledge, the level of precision in image guidance described in this paper has not been reported previously.

While some studies have reported ultrasound-evoked responses, recent work has comprehensively examined the effect of ultrasound excitation in rodent models in which a thin but long ultrasound focus extends throughout the skull base. [26,27] These large ultrasound foci appear to interact with the skull base, where the mechanical transduction system of the ear is rigidly housed. While surgical or chemical destruction of the auditory nerve may help remove this bias, the DMUA avoids focused insonation of the skull base, ameliorating auditory startle responses. Ultrasound delivered by a phased array is spread over a much larger surface of the skull, and we have never observed a response from the rodents during experiments. Based on *in vivo* characterization of the tFUS-induced heating and mechanical focus, we can state confidently that no significant thermal or mechanical energy was delivered distal to the target. This was a major design goal in choosing the operating frequency and geometry of the transducer. In contrast, prefocal heating is a characteristic of the exposures used in this study, heating brain tissues proximal to the target. The extent of the affected brain tissue volume depends on the actual exposure duration and the duty cycle, but it is safe to state that the affected volume has a pyramid shape extending from just below the cortex with an apex at the target. As a result, thermal suppression of the

Author Manuscript Author Manuscript Author Manuscript Author Manuscript

SSEP may be a result of white matter and/or gray matter suppression from the thalamus to the cortex. Further refinement of the affected volume can be achieved by refocusing the tFUS beam to compensate for distortion through the skull, as well as site-specific design of DMUA arrays, both part of our ongoing research.

While excitation of electrophysiologic potential by ultrasound was not observed in this study, we did observe reproducible suppression of the SSEP that was dose dependent on the US intensity. Combinations of amplitude and duty cycle were tested while holding the intensity constant and suppression was found to be related only to the total energy delivered. Ultrasound inhibition was measured by peak-to-peak SSEP amplitude normalized to the baseline. Inhibition was found to be sigmoidally related to the time average ultrasound intensity. The effect of FUS took tens of seconds to achieve maximal effect, and persisted for tens of seconds after cessation of the therapy.

Others have previously reported inhibition with ultrasound, here we rigorously explored this effect and found that it depended primarily on intensity (I_{SPTA}), rather than the pressure-wave amplitude or duty cycle. Previous reports have discounted the role of temperature in neuroinhibition. [3,25,37–39] Despite the common practice of differentiating thermal from non-thermal effects of ultrasound, these effects are interdependent, as others have highlighted. [40] Some reports have dismissed the role of temperature using MR thermometry, which has a thermal resolution of 1–2° C. [23] In the present work, saturated SSEP suppression was achieved with temperature changes of approximately 2°, measured with ultrasound thermography and fine w ire thermocouples with 0.1° C resolution. We demonstrate that the temperature produced at the focus is highly correlated with the ultrasound intensity, and the time course of suppression was similar to the thermal time constant observed during ultrasound heating, suggesting that temperature played a causal or necessary role. These intensities are far below the threshold for transient cavitation at 3.2 MHz. While stable cavitation cannot be ruled out due to the lack of a threshold, DMUA imaging did not detect microbubble activity at these exposure levels *in vivo*. To isolate the effect of thermal energy on SSEPs, we used laser heating with a similar heating profile as a cross-modal method of validation. Despite an inherently different mechanism of heating, the effect on the SSEP was significant and similar to fUS, confirming our hypothesis that thermal energy plays a central role in focused ultrasound neuromodulation. While other effects may play a role in the suppression of neural activity, we believe this work provides strong evidence that much of the suppression can be attributed to thermal neuromodulation.

Thermal neuromodulation in a restricted focus through a noninvasive method offers a promising platform for translation into research and clinical practice for diseases of the central nervous system. Existing knowledge about the safety of thermal energy as a therapy should encourage translational application of thermal ultrasound neuromodulation to treat functional diseases of the nervous system in addition to its use for brain mapping. Noninvasive tFUS is not restricted to a single focus and is well-poised for closed-loop and stereotactic application. Noninvasively heating a spatially-restricted volume of neural tissue without damage may provide a method of controlling or influencing networks through multiple foci and investigating the basis of disease and neural function.

Author Manuscript Author Manuscript Author Manuscript Author Manuscript

Supplementary Material

Refer to Web version on PubMed Central for supplementary material.

Acknowledgements

We would like to acknowledge Brent Clark, MD, PhD, Flaviu Tabaran, DVM, PhD, and Gerrald O'Sullivan, MVB, PhD for their expertise and help with histology.

Sources of funding

This work was funded by the United States National Institutes of Health National Institute of Neurological Disorders and Stroke (NINDS) R01 NS098781 and University of Minnesota MNDrive Neuromodulation.

References

[1]. Fry FJ, Ades HW, Fry WJ. Production of reversible changes in the central nervous system by ultrasound. Science 1958;127:83–4. [PubMed: 13495483]

[2]. Baek H, Pahk KJ, Kim H. A review of low-intensity focused ultrasound for neuromodulation. Biomed Eng Lett 2017;7:135–42. [PubMed: 30603160]

[3]. Naor O, Krupa S, Shoham S. Ultrasonic neuromodulation. J Neural Eng 2016;13:031003. [PubMed: 27153566]

[4]. Darrow DP. Focused ultrasound for neuromodulation. Neurotherapeutics 2019;16:88–99. [PubMed: 30488340]

[5]. Haritonova A, Liu D, Ebbini ES. In Vivo application and localization of transcranial focused ultrasound using dual-mode ultrasound arrays. IEEE Trans Ultrason Ferroelectr Freq Control 2015;62:2031–42. [PubMed: 26670845]

[6]. Kyriakou A, Neufeld E, Werner B, Paulides MM, Szekely G, Kuster N. A review of numerical and experimental compensation techniques for skull-induced phase aberrations in transcranial focused ultrasound. Int J Hyperth 2014;30:36–46.

[7]. Hynynen K, Clement GT, McDannold N, Vykhodtseva N, King R, White PJ, et al. 500-element ultrasound phased array system for noninvasive focal surgery of the brain: a preliminary rabbit study with ex vivo human skulls. Magn Reson Med 2004;52:100–7. [PubMed: 15236372]

[8]. Legon W, Ai L, Bansal P, Mueller JK. Neuromodulation with single-element transcranial focused ultrasound in human thalamus. Hum Brain Mapp 2018;39:1995–2006. [PubMed: 29380485]

[9]. Casper AJ, Liu D, Ballard JR, Ebbini ES. Real-time implementation of a dual-mode ultrasound array system: in vivo results. IEEE (Inst Electr Electron Eng) Trans Biomed Eng 2013;60:2751–9.

[10]. Ballard JR, Casper AJ, Liu D, Haritonova A, Shehata IA, Troutman M, et al. Dual-mode ultrasound arrays for image-guided targeting of atheromatous plaques. In: AIP Conference Proceedings, 1503 AIP; 2012 p. 124–8.

[11]. Ebbini ES, Yao H, Shrestha A. Dual-mode ultrasound phased arrays for image-guided surgery. Ultrason Imaging 2006;28:65–82. [PubMed: 17094688]

[12]. Bayat M, Ballard JR, Ebbini ES. Ultrasound thermography in vivo: a new model for calculation of temperature change in the presence of temperature heterogeneity. In: IEEE international ultrasonics symposium (IUS) ieeexplore.ieee.org; 2013; 2013 p. 116–9.

[13]. Khanna N, Gandhi D, Steven A, Frenkel V, Melhem ER. Intracranial applications of MR imaging–guided focused ultrasound. AJNR Am J Neuroradiol 2016 10.3174/ajnr.A4902.

[14]. Krishna V, Sammartino F, Agrawal P, Changizi BK, Bourekas E, Knopp MV, et al. Prospective tractography-based targeting for improved safety of focused ultrasound thalamotomy. Neurosurgery 2018 10.1093/neuros/nyy020.

[15]. Mueller J, Legon W, Opitz A, Sato TF, Tyler WJ. Transcranial focused ultrasound modulates intrinsic and evoked EEG dynamics. Brain Stimul 2014;7:900–8. [PubMed: 25265863]

Author Manuscript Author Manuscript Author Manuscript Author Manuscript

[16]. Kim H, Park MY, Lee SD, Lee W, Chiu A, Yoo S-S. Suppression of EEG visual-evoked potentials in rats through neuromodulatory focused ultrasound. Neuroreport 2015;26:211–5. [PubMed: 25646585]

[17]. Legon W, Bansal P, Tyshynsky R, Ai L, Mueller JK. Transcranial focused ultrasound neuromodulation of the human primary motor cortex. Sci Rep 2018;8:10007. [PubMed: 29968768]

[18]. Gulick DW, Li T, Kleim JA, Towe BC. Comparison of electrical and ultrasound neurostimulation in rat motor cortex. Ultrasound Med Biol 2017;43:2824–33. [PubMed: 28964613]

[19]. Kamimura HAS, Wang S, Chen H, Wang Q, Aurup C, Acosta C, et al. Focused ultrasound neuromodulation of cortical and subcortical brain structures using 1.9 MHz. Med Phys 2016;43:5730. [PubMed: 27782686]

[20]. Mehić E, Xu JM, Caler CJ, Coulson NK, Moritz CT, Mourad PD. Increased anatomical specificity of neuromodulation via modulated focused ultrasound. PLoS One 2014;9:e86939. [PubMed: 24504255]

[21]. Yang P-F, Phipps MA, Newton AT, Chaplin V, Gore JC, Caskey CF, et al. Neuromodulation of sensory networks in monkey brain by focused ultrasound with MRI guidance and detection. Sci Rep 2018;8:7993. [PubMed: 29789605]

[22]. Fisher JAN, Gumenchuk I. Low-intensity focused ultrasound alters the latency and spatial patterns of sensory-evoked cortical responses in vivo. J Neural Eng 2018;15:035004. [PubMed: 29436519]

[23]. Dallapiazza RF, Timbie KF, Holmberg S, Gatesman J, Lopes MB, Price RJ, et al. Noninvasive neuromodulation and thalamic mapping with low-intensity focused ultrasound. J Neurosurg 2017;1–10.

[24]. Daniels D, Sharabi S, Last D, Guez D, Salomon S, Zivli Z, et al. Focused ultrasound-induced suppression of auditory evoked potentials in vivo. Ultrasound Med Biol 2018;44:1022–30. [PubMed: 29501283]

[25]. Tufail Y, Matyushov A, Baldwin N, Tauchmann ML, Georges J, Yoshihiro A, et al. Transcranial pulsed ultrasound stimulates intact brain circuits. Neuron 2010;66:681–94. [PubMed: 20547127]

[26]. Sato T, Shapiro MG, Tsao DY. Ultrasonic neuromodulation causes Widespread cortical activation via an indirect auditory mechanism. Neuron 2018;98 1031–41.e5. [PubMed: 29804920]

[27]. Guo H, Hamilton M 2nd, Offutt SJ, Gloeckner CD, Li T, Kim Y, et al. Ultrasound produces extensive brain activation via a cochlear pathway. Neuron 2018;98 1020–30.e4. [PubMed: 29804919]

[28]. ter Haar G. Therapeutic applications of ultrasound. Prog Biophys Mol Biol 2007;93:111–29. [PubMed: 16930682]

[29]. Wan Y, Ebbini ES. Imaging with concave large-aperture therapeutic ultrasound arrays using conventional synthetic-aperture beamforming. IEEE Trans Ultrason Ferroelectr Freq Control 2008;55:1705–18. [PubMed: 18986915]

[30]. Ebbini ES, Simon C, Liu D. Real-time ultrasound thermography and thermometry [life sciences]. IEEE Signal Process Mag 2018;35:166–74. [PubMed: 30283214]

[31]. Liu D, Schaible K, Low W, Ebbini ES. Three-dimensional image guidance for transcranial focused ultrasound therapy. In: IEEE 14th international symposium on biomedical imaging (ISBI 2017) ieeexplore.ieee.org; 2017; 2017 p. 916–9.

[32]. Paxinos G, Watson C. The rat brain atlas in stereotaxic coordinates. San Diego: Academic; 1998.

[33]. Patel YA, George A, Dorval AD, White JA, Christini DJ, Butera RJ. Hard real-time closed-loop electrophysiology with the Real-Time eXperiment Interface (RTXI). PLoS Comput Biol 2017;13:e1005430. [PubMed: 28557998]

[34]. White J, Clement GT, Hynynen K. Transcranial ultrasound focus reconstruction with phase and amplitude correction. IEEE Trans Ultrason Ferroelectr Freq Control 2005;52:1518–22. [PubMed: 16285450]

[35]. Sakatani K, Iizuka H, Young W. Somatosensory evoked potentials in rat cerebral cortex before and after middle cerebral artery occlusion. Stroke 1990;21:124–32. [PubMed: 2300979]

Author Manuscript Author Manuscript Author Manuscript Author Manuscript

[36]. Min B-K, Bystritsky A, Jung K-I, Fischer K, Zhang Y, Maeng L-S, et al. Focused ultrasound-mediated suppression of chemically-induced acute epileptic EEG activity. BMC Neurosci 2011;12:23. [PubMed: 21375781]

[37]. Yoo S-S, Bystritsky A, Lee J-H, Zhang Y, Fischer K, Min B-K, et al. Focused ultrasound modulates region-specific brain activity. Neuroimage 2011;56: 1267–75. [PubMed: 21354315]

[38]. Kim H, Taghados SJ, Fischer K, Maeng L-S, Park S, Yoo S-S. Noninvasive transcranial stimulation of rat abducens nerve by focused ultrasound. Ultrasound Med Biol 2012;38:1568–75. [PubMed: 22763009]

[39]. Wright CJ, Rothwell J, Saffari N. Ultrasonic stimulation of peripheral nervous tissue: an investigation into mechanisms. J Phys Conf Ser 2015;581:012003.

[40]. Baker KG, Robertson VJ, Duck FA. A review of therapeutic ultrasound: biophysical effects. Phys Ther 2001;81:1351–8. [PubMed: 11444998]

Author Manuscript Author Manuscript Author Manuscript Author Manuscript

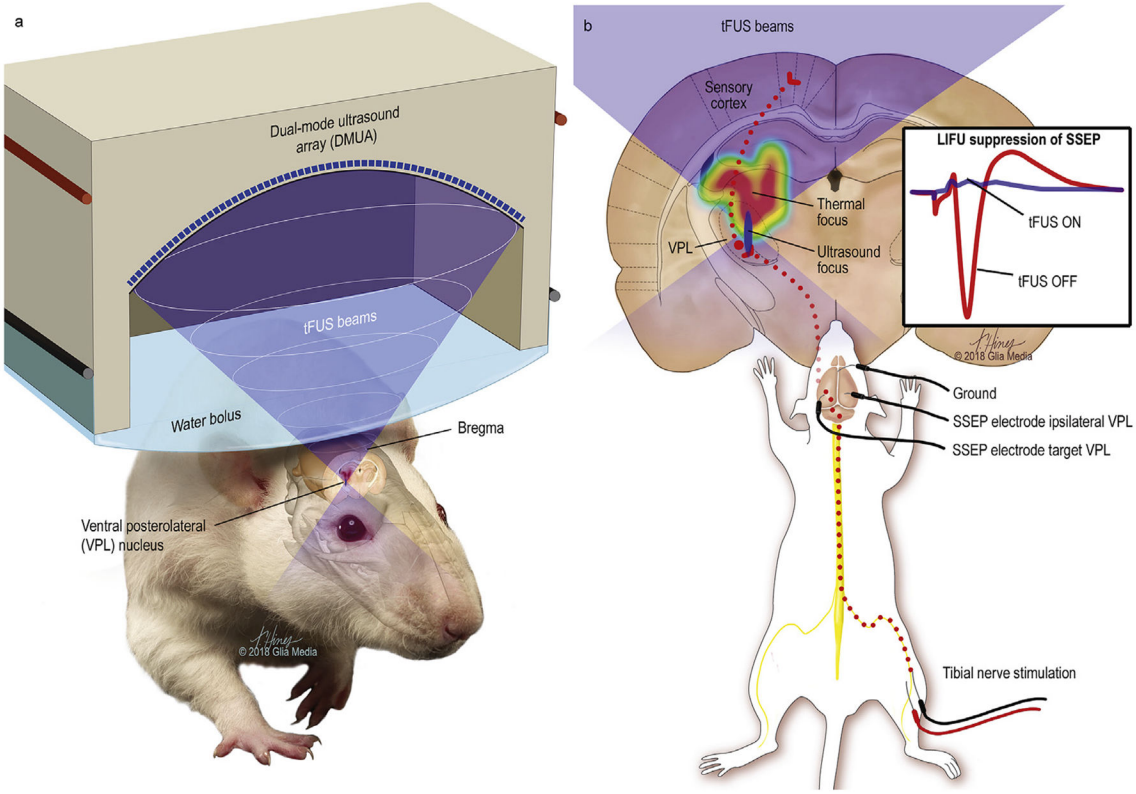

Fig. 1. Transcranial-focused low-intensity ultrasound neuromodulation.

Illustration of the delivery of transcranial focused ultrasound to the ventral posterolateral nucleus of the thalamus with the mechanical focus highlighted in blue and the larger and more proximate heating profile as a color gradient with maximal thermal delivery in red. Electrical stimulation of the tibial nerve produces signals that travel through the nucleus gracilis, followed by the medial lemniscus to the contralateral ventral posterolateral nucleus of the thalamus, which projects to the somatosensory cortex. Evoked somatosensory-evoked potentials (SSEP) from the VPL with and without ultrasound are illustrated (1b inset).

Author Manuscript Author Manuscript Author Manuscript Author Manuscript

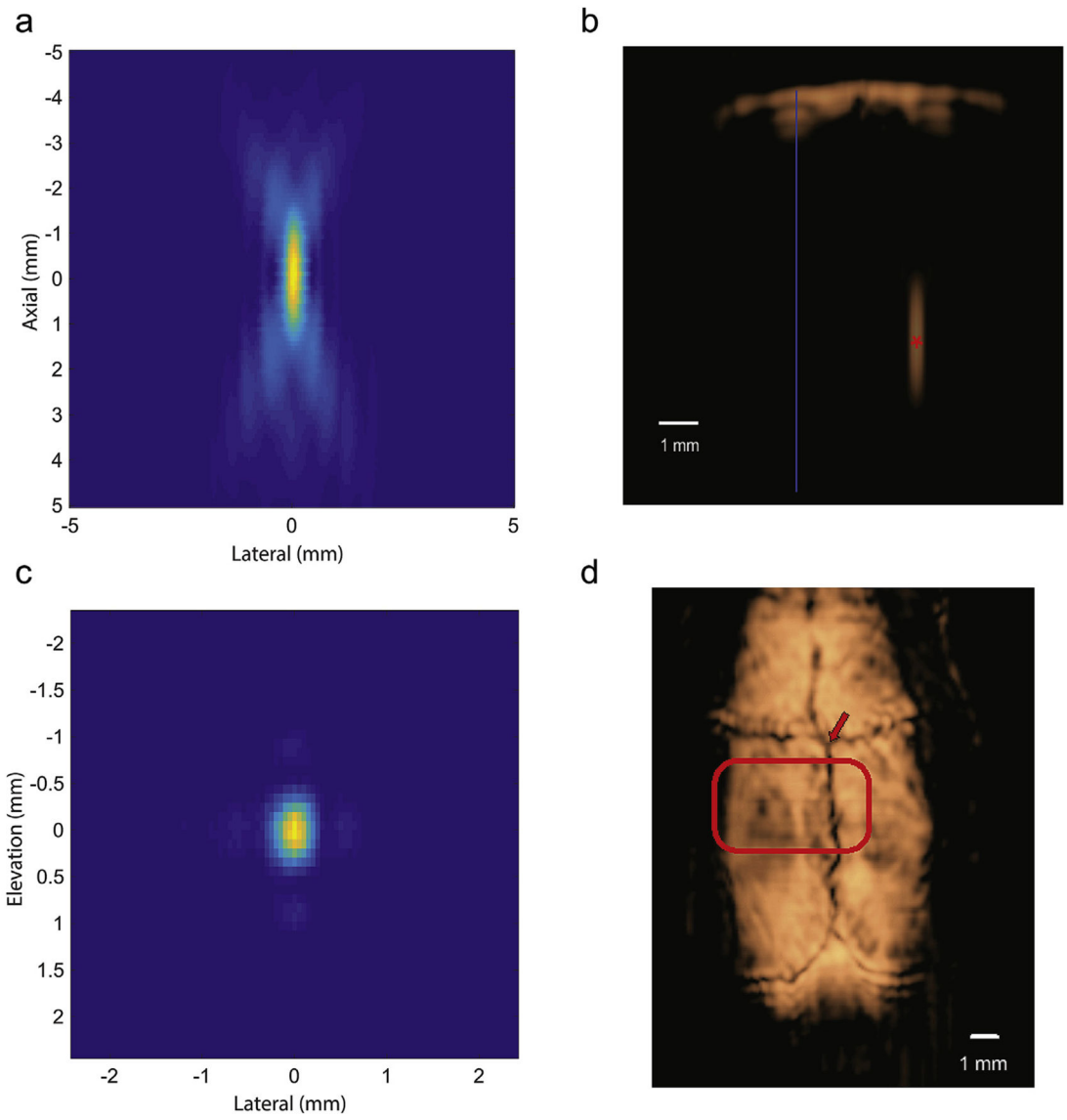

Fig. 2. Image-guided targeting and tFUS beam characterization.

a: Focus measured in degassed water demonstrating the axial extent of the focus (coronal section). b: B-mode image of the skull at 3 mm behind Bregma with the focal spot placement within the brain (6 mm deep) (red asterisk) with midline (blue). c: Focus measured in degassed water demonstrating the lateral-elevation profile (axial section). d: A C-scan image of a rodent skull surface from 3D DMUA imaging with the active ultrasound wavefront highlighted. The DMUA was positioned with respect to the intersection of the bregma and medial suture lines (arrow). The intersection of the bregma and medial suture lines (arrow) served as a marker for placing the DMUA for targeting the stereotactic coordinates. The highlighted region illustrates the cross section of the tFUS beam at the skull surface.

Author Manuscript
Author Manuscript
Author Manuscript
Author Manuscript

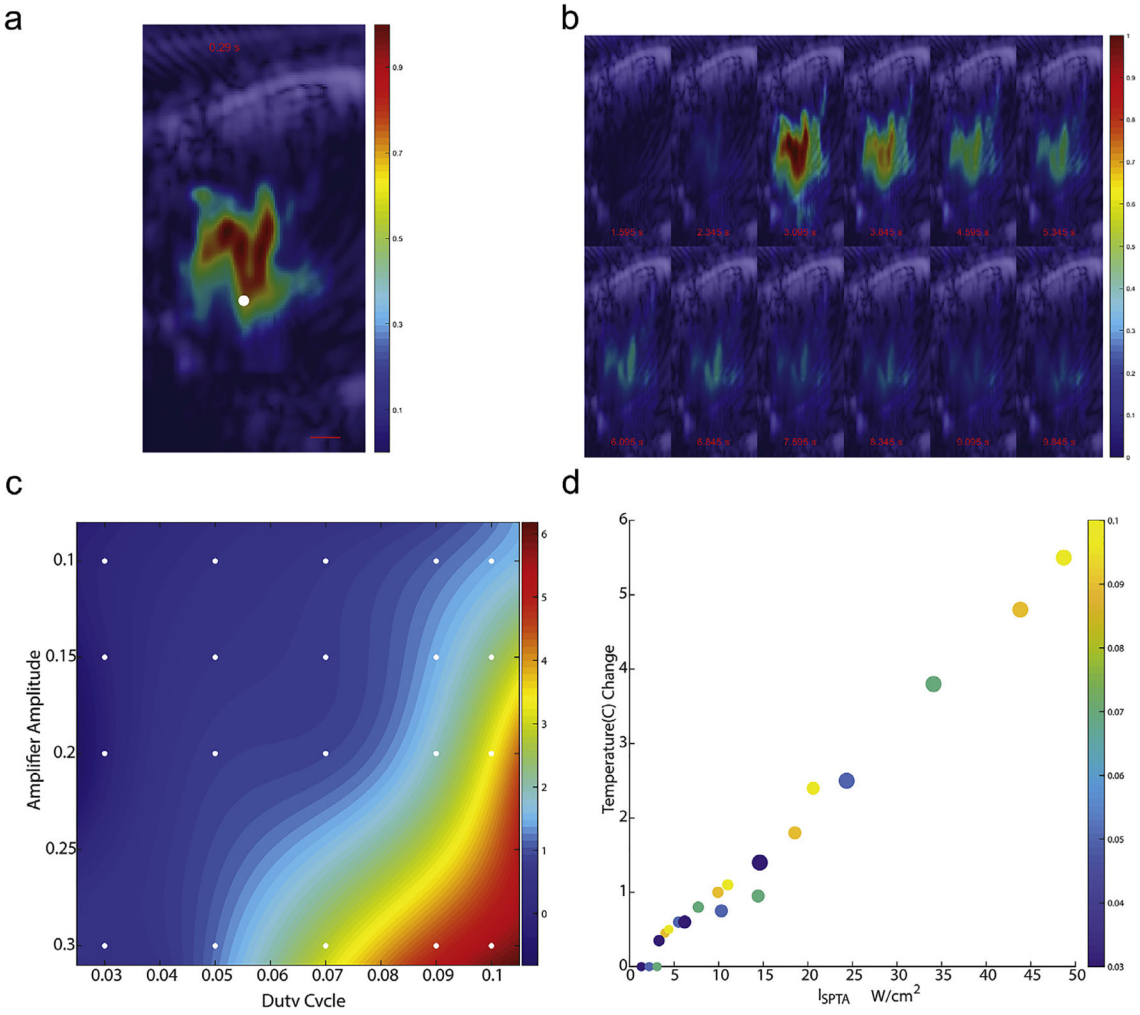

Fig. 3. Temperature field created by TFUS.

a: A spatial profile of the initial heating rate induced by a 1-sec tFUS beam at 50% DC with colorbar indicating temperature in Celsius and white dot at the target focus. b: montage of tFUS-induced temperature profiles at 0.4 s intervals (timestamps with respect to tFUS application at 0 s). The duty cycle of this test shot is 50% rather than the typical 10% c: The interpolated temperature surface of the amplitude-duty cycle parameter space is plotted over a gradient with reference markers indicating the locations of measured steady-state temperature changes from a image-guided thermocouple. d: Steady-state temperature changes are plotted across the corresponding duty cycles (displayed in color) and amplifier amplitudes (size of the marker) against the SPTA intensity.

Author Manuscript Author Manuscript Author Manuscript Author Manuscript

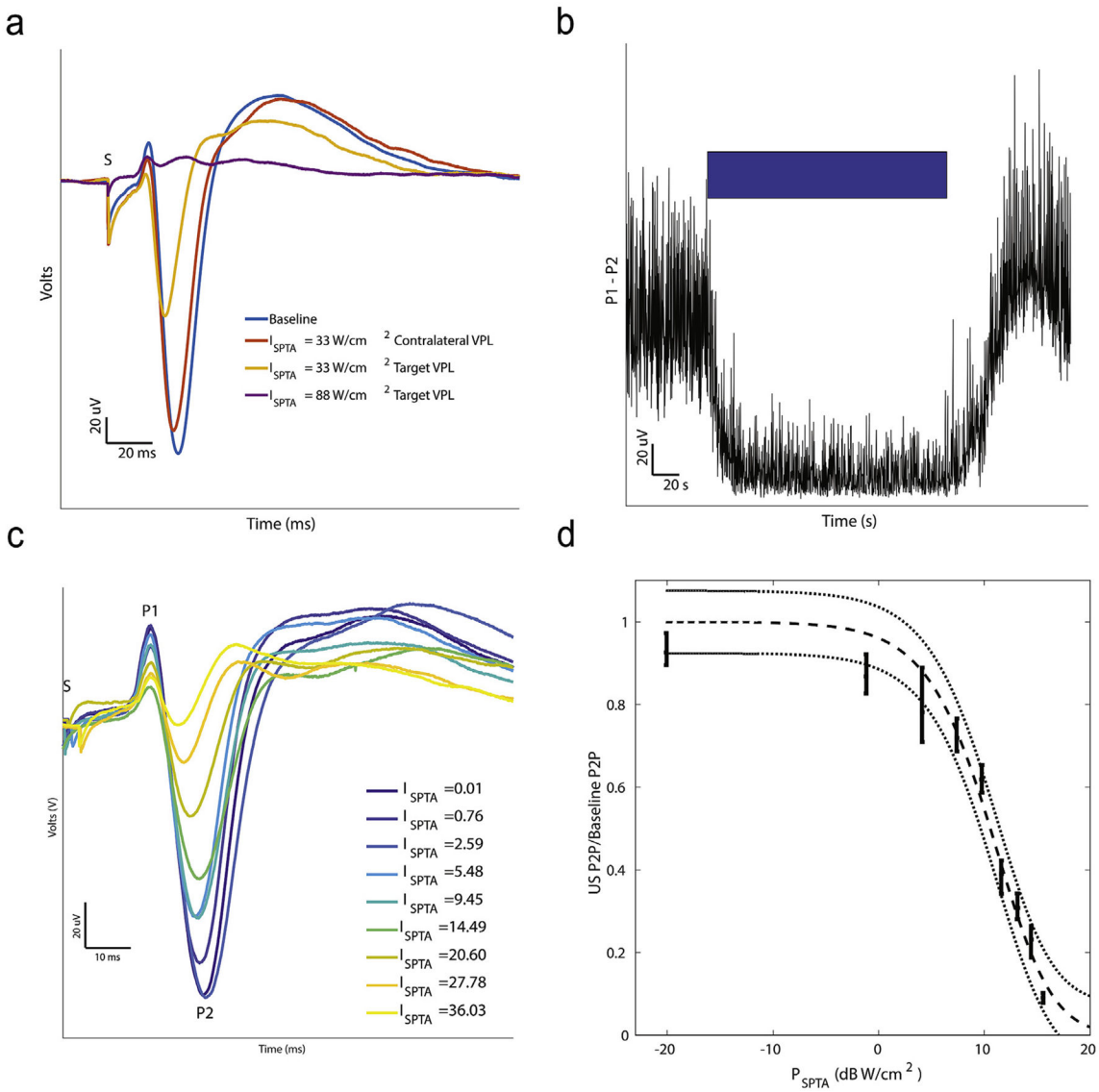

Fig. 4. Effect of tFUS on SSEP waveform.

a: SSEP waveforms for baseline, contralateral VPL, and targeted VPL at two intensities with the three main peaks (P1, P2, and P3) and stimulation artifact (S) truncated. b: Raw Peak-to-Peak (P1 to P2) during the course of an experiment (blue bar indicates time when ultrasound is on). c: (Left) SSEP waveforms are plotted for different ultrasound intensities, measured with I_{SPTA}. d: The ratio of the peak-to-peak SSEP amplitude during ultrasound to baseline plotted against the corresponding SPTA power. Bars indicate means ± standard deviations of the measured peak-to-peak ratios. A sigmoid function fit to the data with 95% confidence intervals is plotted in dashed gray ($R^2 = 0.98$). Electrical stimulation (600 μs) of the tibial nerve was delivered at the zero timepoint denoted in a and c by S where stimulation artifacts are truncated.

Author Manuscript Author Manuscript Author Manuscript Author Manuscript

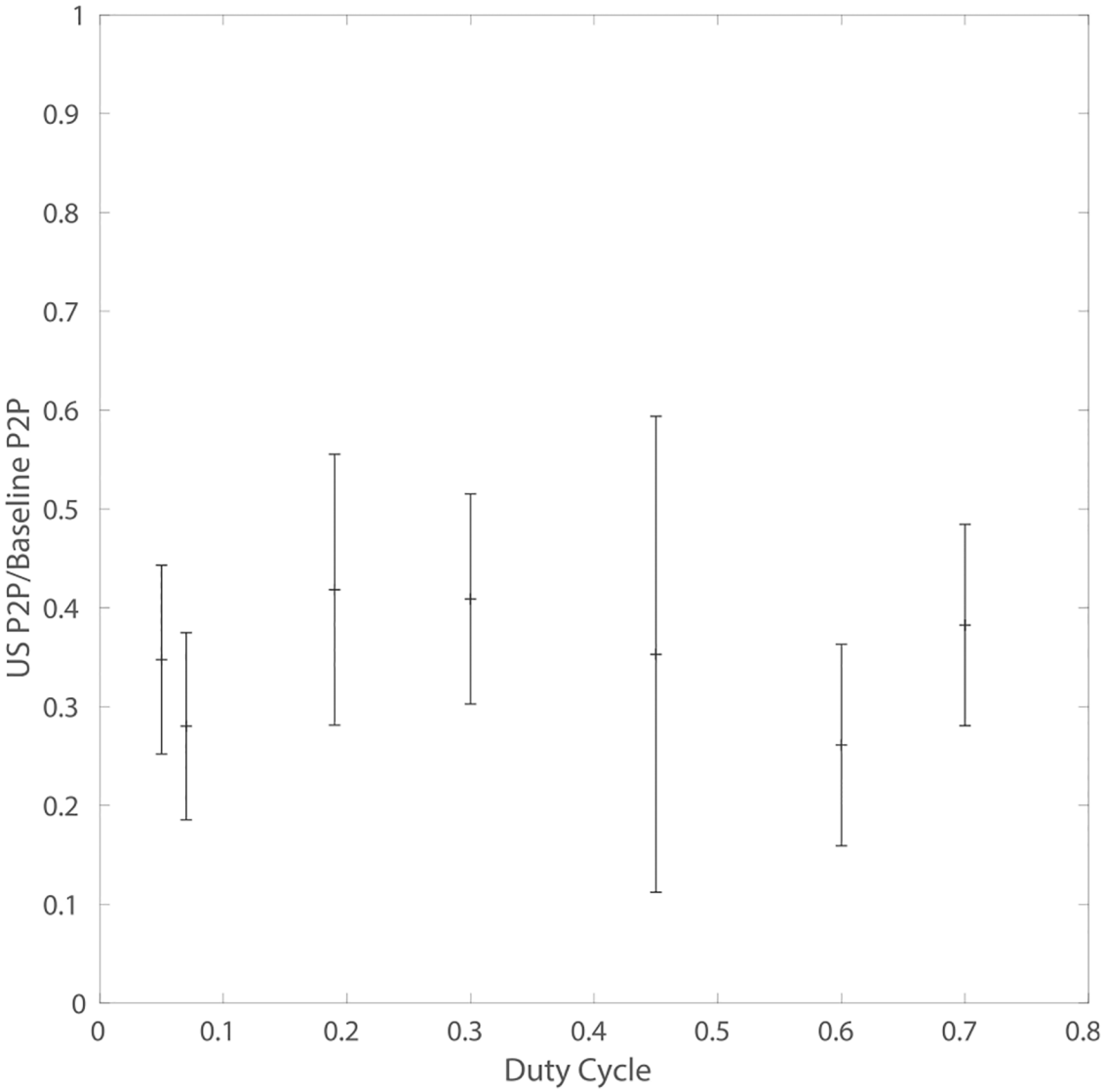

Fig. 5. Ultrasound suppression at a constant I_{SPTA}.

Duty cycle was varied while adjusting the amplitude to hold ISPTA constant at 20 W/cm^2, an energy level that caused approximately 50% reduction in SSEP amplitude. SSEP peak-to-peak relative to mean baseline amplitude with 90% confidence bounds are shown. No significant effect of duty cycle was observed.

Author Manuscript Author Manuscript Author Manuscript Author Manuscript

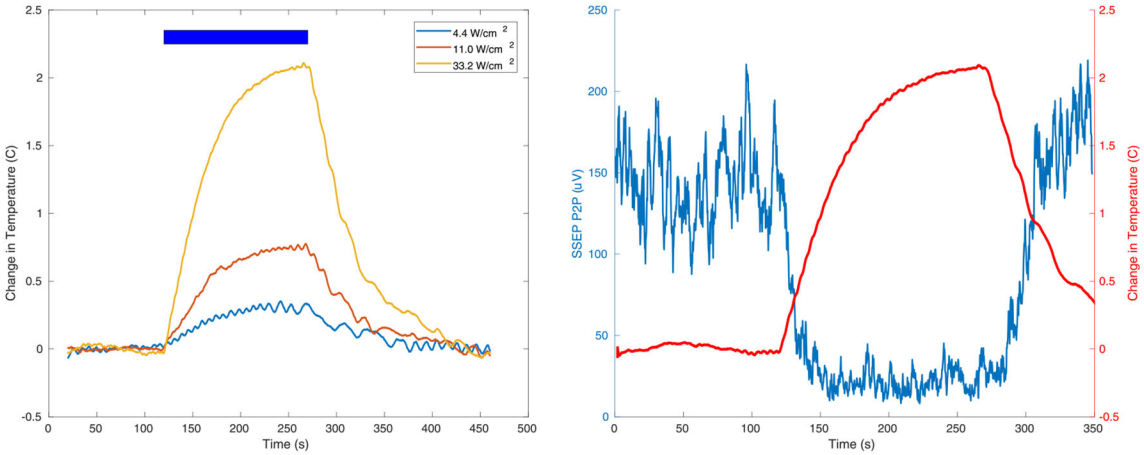

Fig. 6. Time course of ultrasound-generated temperature and SSEP change.

(Left)Tissue temperature increases during ultrasound at three different intensities and recovers to baseline over several 10s of seconds. The blue bar indicates time during ultrasound application. Temperature changes build up with a time constant on the order of 10s of seconds and dissipate with similar time constants. (Right) Simultaneous measurement of temperature and SSEP peak-to-peak suppression with tFUS as a function of time. The blue bar indicates time during which tFUS was applied. The suppression of the SSEP closely follows the temperature effects, suggesting that temperature may be a contributing mechanism for suppressing the SSEP.

Author Manuscript Author Manuscript Author Manuscript Author Manuscript

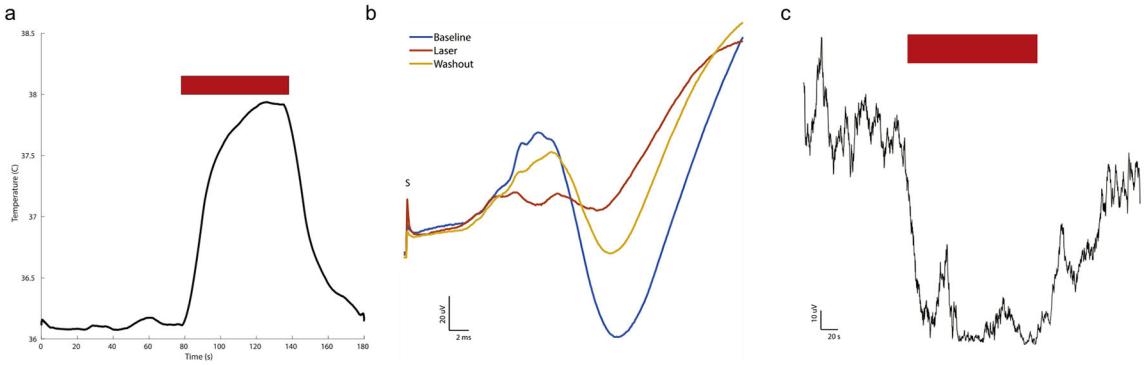

Fig. 7. Laser-mediated thermal neuromodulation.

a: Temperature change caused by laser heating in thalamus at tip of fiberoptic catheter as a function of time. Red bar indicates time when the laser was applied. An approximately 2 °C steady state change is observed within a minute of application of the laser. b: Average SSEP waveform during Baseline, Laser Neuromodulation, and during the Washout or recovery period. c: Peak-to-peak (P1 to P2) of the SSEP during the Laser application. Red bar indicates time when the laser is on. Electrical stimulation (600 μs) of the tibial nerve was delivered at the zero timepoint by S where stimulation artifacts are truncated.